

Received February 23, 2021, accepted March 2, 2021, date of publication March 8, 2021, date of current version March 16, 2021.

Digital Object Identifier 10.1109/ACCESS.2021.3064413

# A Control Strategy of Islanded Microgrid With Nonlinear Load for Harmonic Suppression

QIANG CHEN 

School of Electric Power Engineering, Nanjing Institute of Technology, Nanjing 211167, China

e-mail: qchen1019@foxmail.com

**ABSTRACT** A control strategy of islanded microgrid is proposed in this paper against the harmonic circulation of the inverters and the Point of Common Coupling (PCC) voltage harmonic distortion of the microgrid caused by nonlinear load. The reference voltage of the inverter's outer voltage loop is given by the decoupling control of the fundamental and harmonic components. Virtual synchronous generator (VSG) is adopted in fundamental domain. In harmonic domain, adaptive harmonic compensation and harmonic virtual impedance are applied to obtain the harmonic components of the reference voltage of the outer voltage loop. The hybrid control strategy combining P control and repetitive control in parallel is adopted in the outer voltage loop. Multi-period repetitive control (MPRC) with fast repetitive control (FRC) is adopted to improve the tracking control performance of the main harmonic components of the given reference voltage. Fractional order delay approximated by Lagrange interpolation polynomial FIR filter is applied in MPRC for different repetitive control periods at the fixed sampling period. The output harmonic current of the inverters can be distributed autonomously according to the capacity of the inverters to suppress the harmonic circulation, and the suppression of the PCC voltage harmonic distortion is realized. Simulation based on Matlab/Simulink and hardware-in-loop(HIL) test are carried out, and the results show that the proposed control strategy is effective.

**INDEX TERMS** Islanded microgrid, nonlinear load, decoupling control, adaptive harmonic compensation, multi-period repetitive control (MPRC).


## I. INTRODUCTION

With the increasing tension of traditional energy and the aggravation of environmental problems, distributed generations such as photovoltaics, wind power and fuel cell develop rapidly, and microgrid composed of distributed generation, energy storage and local load is widely used [1]–[3]. Microgrid often contains nonlinear load which leads to the harmonic circulation among the inverters and the PCC voltage harmonic distortion of the microgrid in islanded operation mode [4]–[6]. The harmonic circulation affects the stable operation of the inverters and even damages them, so it is necessary to distribute the output harmonic current among the inverters to suppress the circulation. IEEE standard requires that the total harmonic distortion (THD) of grid voltage should not be more than 5% [7]. When the PCC voltage harmonic of microgrid are serious, it will affect the operation of the electrical equipments in the microgrid. Therefore, the PCC voltage harmonic components caused by nonlinear

load should be suppressed to ensure the power quality of microgrid.

Active power-frequency ( $P$ - $f$ ) and reactive power-voltage magnitude ( $Q$ - $V$ ) droop control is usually applied in the parallel operation of the inverters in islanded microgrid, which can realize the power sharing among the inverters without communication links [8]–[10]. Nevertheless, droop control is only applied in fundamental domain for the sharing of the fundamental power. Due to the harmonic circulation and distortion caused by nonlinear load, it is not effective. Therefore, the sharing of the harmonic current and the suppression of the PCC voltage distortion are focused in this paper.

Applying APF to microgrid can effectively suppress the harmonics [11], but this increases the cost of the microgrid. On the other hand, the harmonic suppression can be realized by the inverter with proper control. The control strategies of the inverter to achieve the harmonic suppression in islanded microgrid are mainly divided into two modes: decentralized autonomous control without communication links and hierarchical control based on communication links [12]. The harmonic circulation among the inverters and the PCC

The associate editor coordinating the review of this manuscript and approving it for publication was Zhilei Yao .

voltage distortion of microgrid are affected by the output impedance of the inverters and the feeder impedance between the inverter and the PCC. Virtual impedance is mostly used for autonomous control without interconnected communication links to achieve the harmonic circulation suppression [12]–[14]. A negative virtual harmonic impedance method was applied in [12] to compensate the effect of feeder impedance on harmonic power delivery. An adaptive virtual impedance control scheme based on small-AC-signal injection was proposed in [13]. The virtual impedance of each inverter was matched for sharing the harmonic power by this method. In [14], the inverter impedance was directly controlled to regulate the output harmonic current of the inverter in islanded microgrid to achieve harmonic current sharing. However, the virtual impedance is needed to be much larger than the feeder impedance for the accurate harmonic current sharing among the inverters, while large virtual impedance leads to the serious PCC voltage distortion. The hierarchical control based on communication links can effectively reduce the influence of the feeder impedance on the harmonic circulation suppression and suppress the PCC voltage harmonic distortion [15]–[17]. Reference [15] adopted central controller to give the harmonic current reference and virtual harmonic admittance of each inverter by communication links according to the detected harmonic contents of the PCC voltage of microgrid. Reference [16] proposed an enhanced virtual harmonic impedance control scheme. According to the rated harmonic power and actual harmonic power of each inverter, the microgrid central controller provided the reference of the harmonic power for each inverter to compensate the mismatch in feeder impedance. Reference [17] adopted hierarchical control which realized a complementary control loop, virtual impedance and harmonic voltage compensation, and power calculation based on harmonic power flow using radial basis function neural network. However, the hierarchical control based on communication links leads to the hardware complexity and reduces the reliability of microgrid, and is also not good for the addition of inverters to expand microgrid. Voltage and current harmonics compensation was realized in [18]. But it's realized by two converters respectively. One is responsible for the voltage harmonic suppression, and the other is used to mitigate the harmonic current.

Proportional resonant control is usually used to realize the closed loop control of each order harmonic component. Resonant controller needs to extract each harmonic component, and the parallel number of resonant controller is limited. So it is difficult to meet the control requirements of each order harmonic, and the control parameters setting is also complex. Repetitive control based on internal model theory can be equivalent to the parallel of integral and each order quasi-resonant control, and the control parameter setting is relatively simple, which can overcome the shortcomings of resonant controller [19], [20].

This paper presents a novel control strategy applied in islanded microgrid with nonlinear load. The inverters in the microgrid can realize the harmonic current distribution and

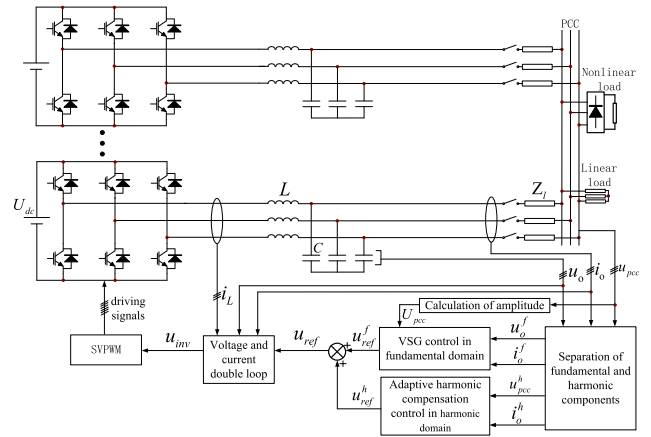


FIGURE 1. Structure of the islanded microgrid with nonlinear load.

the PCC voltage distortion suppression simultaneously in islanded microgrid by autonomous control. The fundamental and harmonic components of the reference voltage of the inverter's voltage loop are obtained by the decoupling control of the fundamental and harmonic components to meet the different control requirements. Virtual inertia and damping are introduced by VSG control in the fundamental droop control. To make up for the deficiencies of virtual impedance, adaptive harmonic compensation and harmonic virtual impedance are combined in the harmonic domain control to suppress the harmonic components of the PCC voltage and the harmonic circulation of the inverters. According to the harmonic characteristics of the three-phase circuit with nonlinear load, the tracking control performance of the main harmonic components is improved by the hybrid control strategy combining P control and MPRC with FRC in parallel.

The sections of this paper are structured as follows. Section II analyses the structure of the islanded microgrid with nonlinear load. Section III presents the VSG control in fundamental domain. Section IV deduces the adaptive harmonic compensation control in harmonic domain. Section V gives the voltage and current double loop control which emphasizes the MPRC. In Section VI, simulation based on Matlab/Simulink and HIL real-time verification test are carried out.

## II. STRUCTURE OF ISLANDED MICROGRID WITH NONLINEAR LOAD

The structure of the islanded microgrid with nonlinear load is shown in Figure 1.  $U_{dc}$  is the dc side voltage of the inverter.  $L$  and  $C$  are the filter inductance and capacitor of the inverter respectively.  $i_L$  is the current of the filter inductance.  $i_o$  is the output current of the inverter. The terminal voltage of  $C$  is  $u_o$  which is the output voltage of the inverter.  $Z_l$  is the feeder impedance between the inverter and the PCC.  $u_{ref}$  is the reference voltage value of the voltage loop.  $u_{inv}$  is the output of the inverter bridge.  $u_{pcc}$  is the PCC voltage.  $U_{pcc}$  is the magnitude of  $u_{pcc}$ .  $i_o^f$  is the fundamental components of

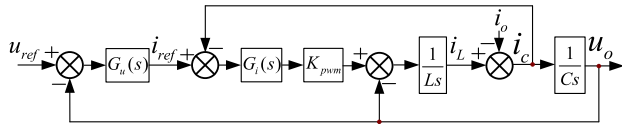


FIGURE 2. Block diagram of the voltage and current double loop.

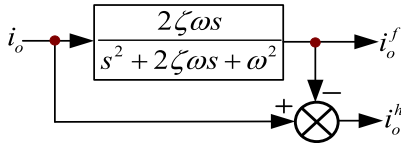


FIGURE 3. Separation method of the fundamental and harmonic components.

$i_o$ . The fundamental components of the physical quantities in this paper are all with superscript  $f$ .  $i_o^h$  is the harmonic components of  $i_o$ . The harmonic components of the physical quantities in this paper are all with superscript  $h$ .

The voltage and current double loop control of the inverter is shown in Figure 2.  $G_u(s)$  is the voltage loop regulator.  $G_i(s)$  is the current loop regulator.  $i_{ref}$  is the reference current value of the current loop.  $i_c$  is the current value of the capacitor  $C$ .  $K_{pwm}$  is the gain of the inverter-bridge.

According to Figure 2, the output voltage of the inverter is expressed by

$$u_o(s) = G(s)u_{ref} - Z_o(s)i_o(s) \quad (1)$$

where  $G(s)$  is the closed-loop transfer function, and  $Z_o$  is the output impedance of the inverter as follows

$$G(s) = \frac{G_i(s)G_u(s)}{LCs^2 + G_i(s)Cs + G_i(s)G_u(s)} \quad (2)$$

$$Z_o(s) = \frac{Ls + G_i(s)}{LCs^2 + G_i(s)Cs + G_i(s)G_u(s)} \quad (3)$$

$i_o$  is decomposed into the fundamental and harmonic components as follows

$$i_o = i_o^f + i_o^h \quad (4)$$

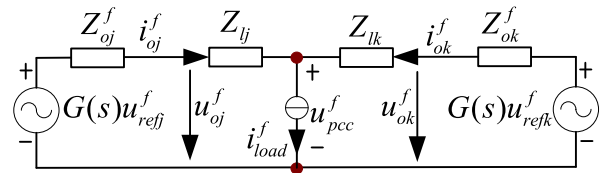
As shown in Figure 3, the separation of the fundamental and harmonic components of  $i_o$  is achieved by band-pass filter.  $\zeta$  is the damping coefficient.  $\omega$  is the actual value of the fundamental electric angular velocity of the inverter.

By substituting (4) into (1), the fundamental and harmonic components of the inverter's output voltage are respectively expressed as

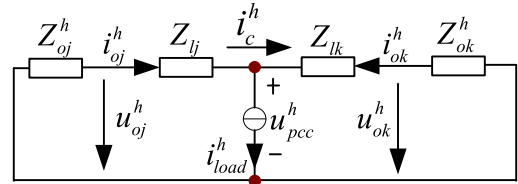
$$u_o^f(s) = G(s)u_{ref}^f - Z_o^f(s)i_o^f(s) \quad (5)$$

$$u_o^h(s) = -Z_o^h(s)i_o^h(s) \quad (6)$$

where  $Z_o^f$  and  $Z_o^h$  are the output impedance of the inverter respectively in fundamental and harmonic domains.  $u_{ref}^f$  and  $u_{ref}^h$  are the fundamental and harmonic components of the reference voltage of the voltage loop respectively.  $Z_o^f = Z_o^h = Z_o$ ,  $u_{ref} = u_{ref}^f + u_{ref}^h$ ,  $u_{ref}^h = 0$ .



(a)



(b)

FIGURE 4. Equivalent circuit of the islanded microgrid: (a) Fundamental domain; (b) Harmonic domain.

According to (5), (6) and Figure 1, the equivalent circuit of the islanded microgrid is shown in Figure 4. The load is equivalent to a current source.  $i_{load}$  is the current of the load. Subscript  $j$  and  $k$  represent the  $j$ th and  $k$ th inverters respectively.  $i_c^h$  is the harmonic circulation.

The rated power ratio of the  $j$ th and  $k$ th inverters is  $w$ . According to Figure 4(b), the harmonic components of the PCC voltage and the harmonic circulation between the two inverters are expressed by

$$u_{pcc}^h = -(Z_{lj} + Z_{oj}^h)i_{oj}^h = -(Z_{lk} + Z_{ok}^h)i_{ok}^h \quad (7)$$

$$i_c^h = \frac{1}{w+1}i_{oj}^h - \frac{w}{w+1}i_{ok}^h = \frac{[(Z_{lk} + Z_{ok}^h) - w(Z_{lj} + Z_{oj}^h)]i_{load}^h}{(w+1)[(Z_{lk} + Z_{ok}^h) + (Z_{lj} + Z_{oj}^h)]} \quad (8)$$

Excessive  $Z_o^h$  results in the harmonic distortion of  $u_{pcc}$  exceeding the standard from (7). But too small  $Z_o^h$  is not conducive to the suppression of the harmonic circulation between the inverters from (8). The effective suppression of  $i_c^h$  and  $u_{pcc}^h$  should be taken into account in the inverter control simultaneously. What's more, the output impedance in harmonic domain needs to be resistive for the distribution of the harmonic current. Therefore, the characteristics of the output impedance in harmonic domain should be different from those for droop control in fundamental domain.

It is shown from (5) and (6) that the output impedance of the traditional control of inverter is the same in fundamental and harmonic domains. So it is difficult to meet the different control requirements of the fundamental and harmonic components, and the control effect with nonlinear load is not ideal. In this paper, the decoupling control of the fundamental and harmonic components is used to obtain the fundamental and harmonic components of the reference voltage of the outer voltage loop to improve the output characteristics of the inverters and the stable operation ability of the islanded microgrid with nonlinear load.

### III. VSG CONTROL IN FUNDAMENTAL DOMAIN

To improve the stability of the droop control in fundamental domain,  $u_{ref}^f$  is given by VSG control to simulate the rotor motion and stator excitation regulation characteristics of synchronous generator so that the frequency and voltage regulation characteristics of the inverter is similar to those of synchronous generator.

According to the decoupling control principle, the power loop of the VSG control adopts the following instantaneous active and reactive power of the inverter in fundamental domain

$$\begin{bmatrix} P^f \\ Q^f \end{bmatrix} = \frac{3}{2} \begin{bmatrix} u_{od}^f & u_{oq}^f \\ u_{oq}^f & -u_{od}^f \end{bmatrix} \begin{bmatrix} i_{qd}^f \\ i_{oq}^f \end{bmatrix} \quad (9)$$

where  $u_{od}^f$  and  $u_{oq}^f$  are the  $dq$  components of  $u_o^f$  respectively, and the  $dq$  components of other physical quantities are expressed by reference to this.

By simulating the primary frequency modulation characteristics, rotor motion equation and stator excitation regulation characteristics of synchronous motor, the VSG control equations are expressed by

$$\begin{cases} P_{ref} = P_0 + k_\omega(\omega_0 - \omega) \\ J \frac{d\omega}{dt} = \frac{P_{ref}}{\omega_0} - \frac{P^f}{\omega_0} - D(\omega - \omega_0) \\ U_{ref} = U_0 + n_Q(Q_0 - Q^f) + k_u(U_0 - U_{pcc}) \end{cases} \quad (10)$$

where  $P_0$  is the rated active power,  $k_\omega$  is the active power droop coefficient,  $P_{ref}$  is the active power reference value,  $\omega_0$  is the rated electrical angular velocity,  $J$  is the moment of inertia,  $D$  is the damping coefficient,  $U_0$  is the rated voltage magnitude,  $n_Q$  is the reactive power droop coefficient,  $Q_0$  is the rated reactive power,  $U_{ref}$  is the voltage magnitude reference value, and  $k_u$  is the regulation coefficient of the PCC voltage.

According to (10), the voltage reference value in fundamental domain given by the VSG control is expressed by

$$u_{ref}^* = \begin{bmatrix} U_{ref} \sin \theta \\ U_{ref} \sin(\theta - 2\pi/3) \\ U_{ref} \sin(\theta - 4\pi/3) \end{bmatrix} \quad (11)$$

where  $\theta$  is the phase angle of the inverter.  $\theta = \int_0^t \omega dt + \varphi$ .  $\varphi$  is the initial phase angle of the inverter.

In order to suppress the current circulation of the inverters in fundamental domain and enhance the stability of the system, the fundamental virtual impedance  $Z_v^f$  is adopted to improve the output characteristics of the inverter. The fundamental components of the reference voltage of the voltage loop is given as

$$u_{ref}^f = -L_v^f \frac{di_o^f}{dt} - R_v^f i_o^f + u_{ref}^* \quad (12)$$

where  $Z_v^f = R_v^f + j\omega L_v^f$ . In order to improve the droop characteristics of the inverter,  $Z_v^f$  needs to be highly inductive.

Based on the above analysis, the control system block diagram of the VSG control in fundamental domain is shown in Figure 5.

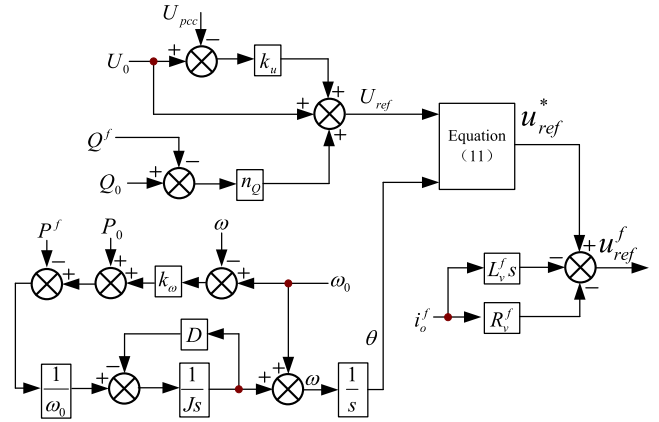


FIGURE 5. Control system block diagram of the VSG control in fundamental domain.

### IV. ADAPTIVE HARMONIC COMPENSATION CONTROL IN HARMONIC DOMAIN

According to (7), the harmonic current of the inverter is determined by the harmonic components of the PCC voltage, the output impedance of the inverter in harmonic domain and the feeder impedance. In order to realize the harmonic current distribution among the inverters, according to Figure 4(b), the harmonic virtual impedance should be resistive,  $Z_v^h = R_v^h$ . The harmonic components of the reference voltage of the voltage loop and the output impedance in harmonic domain are respectively expressed by

$$u_{ref}^h = -R_v^h i_o^h \quad (13)$$

$$Z_o^h(s) = \frac{Ls + G_i(s)}{LCs^2 + G_i(s)Cs + G_i(s)G_u(s)} + R_v^h G(s) \quad (14)$$

According to (6), (8) and (14),  $R_v^h$  and  $Z_l$  affect the distribution of the harmonic current together. In order to ensure the distribution effect of the harmonic current,  $R_v^h \gg Z_l$  to ignore the effect of  $Z_l$ . Although increasing  $R_v^h$  can improve the control performance of the harmonic current distribution, it also increases the harmonic components of the inverter's output voltage which leads to the aggravation of the PCC voltage harmonic distortion and affects the power quality of the microgrid. For the harmonic suppression of the PCC voltage, a harmonic compensation loop is introduced. According to Figure 4(b), the harmonic compensation loop is given as

$$U_h = -u_{pcc}^h k_h \quad (15)$$

where  $k_h$  is the harmonic compensation coefficient.  $u_{ref}^h$  is adjusted as

$$u_{ref}^h = U_h - R_v^h i_o^h \quad (16)$$

According to Figure 4(b), it has

$$u_{pcc}^h = u_o^h - Z_l i_o^h \quad (17)$$

(17) is substituted into (16),  $u_{ref}^h$  and  $Z_o^h$  is adjusted as

$$u_{ref}^h = (Z_l i_o^h - u_o^h) k_h - R_v^h i_o^h \quad (18)$$

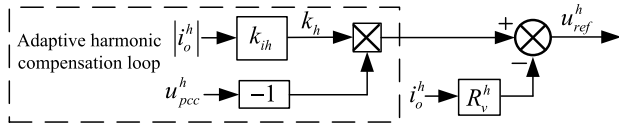


FIGURE 6. Adaptive harmonic compensation control.

$$Z_o^h(s) = \frac{(Ls + G_i(s))/(1 + k_h G(s))}{LCs^2 + G_i(s)Cs + G_i(s)G_u(s)} + \frac{(R_v^h - k_h Z_l)G(s)}{1 + k_h G(s)} \quad (19)$$

Then combining (7), according to the final value theorem  $u_{pcc}^h$  in steady-state is given as

$$u_{pcc}^h(\infty) = -\frac{R_v^h + Z_l}{1 + k_h} i_o^h \quad (20)$$

In (20),  $u_{pcc}^h$  is inverse proportional to  $k_h$ . Too small  $k_h$  is not conducive to suppress the harmonic components of the PCC voltage, but it is shown from (19) that excessive  $k_h$  reduces the shunt effect of  $R_v^h$  and affect the harmonic current distribution. What's more,  $u_{pcc}^h$  is proportional to  $i_o^h$ . For the harmonic compensation loop can meet the demand of the PCC voltage distortion suppression and the harmonic current distribution simultaneously, adaptive harmonic compensation control is introduced in this paper as follows

$$k_h = k_{ih} \left| \frac{i_o^h}{i_o^h} \right| \quad (21)$$

where  $k_{ih}$  is the adaptive harmonic compensation coefficient. Adaptive harmonic compensation control is shown in Figure 6.

As shown in Figure 6,  $i_o^h$  is proportionate to  $k_h$ . Since the effect of  $k_h$  on  $u_{pcc}^h$  is the opposite of the effect of  $i_o^h$ , adaptive control can reduce the effect of  $i_o^h$  on  $u_{pcc}^h$  and effectively realize the suppression of  $u_{pcc}^h$ . Setting  $k_{ih}$  in a reasonable value can ensure the distribution effect of the harmonic current.

IEEE standard stipulates that the PCC voltage THD should not be more than 5% as

$$\left| \frac{u_{pcc}^h}{u_{pcc}^f} \right| \leq \left| \frac{u_{pcc}^f}{u_{pcc}^f} \right| \cdot 5\% \quad (22)$$

Substitute (20) and (21) into (22),  $\left| \frac{u_{pcc}^h}{u_{pcc}^f} \right|$  and  $\left| \frac{i_o^h}{i_o^h} \right|$  respectively take the rated voltage and current magnitude of the inverter, and  $R_v^h \gg Z_l$ , so  $k_{ih}$  is given as

$$k_{ih} \geq \frac{R_v^h}{0.05U_0} - \frac{1}{I_0} \quad (23)$$

where  $I_0$  is the rated current magnitude of the inverter. For the value of  $Z_l$  is ignored in (23) and the value of  $k_{ih}$  needs to be limited for the harmonic current distribution, the value of  $k_{ih}$  is slightly greater than the value of the right of (23).

To suppress the harmonic circulation among the inverters, the output harmonic current of the inverters should be distributed according to the capacity of each inverter.  $w$  is the ratio of the rated power between the  $j$ th and  $k$ th inverters, then

the harmonic current distribution between the two inverters is given as

$$i_{oj}^h : i_{ok}^h = w \quad (24)$$

Substituting (24) into (20), it has

$$\frac{R_{vj}^h + Z_l}{1 + wk_{ihj} \left| \frac{i_{ok}^h}{i_{ok}^h} \right|} w = \frac{R_{vk}^h + Z_l}{1 + k_{ihk} \left| \frac{i_{ok}^h}{i_{ok}^h} \right|} \quad (25)$$

$R_v^h \gg Z_l$ , then ignoring the influence of  $Z_l$ , it has

$$wR_{vj}^h + wR_{vj}^h k_{ihk} \left| \frac{i_{ok}^h}{i_{ok}^h} \right| = R_{vk}^h + R_{vk}^h w k_{ihj} \left| \frac{i_{ok}^h}{i_{ok}^h} \right| \quad (26)$$

where

$$\begin{cases} R_{vk}^h = wR_{vj}^h \\ k_{ihk} = wk_{ihj} \end{cases} \quad (27)$$

Therefore, the relationship among the rated power, the adaptive compensation coefficient and the harmonic virtual impedance of the inverters is determined by

$$\begin{cases} k_{ih1}S_1 = k_{ih2}S_2 = \dots = k_{ihn}S_n \\ R_{v1}^hS_1 = R_{v2}^hS_2 = \dots = R_{vn}^hS_n \end{cases} \quad (28)$$

where  $R_{vn}^h$ ,  $S_n$  and  $k_{ihn}$  are the harmonic virtual impedance, the rated power and the adaptive harmonic compensation coefficient of the  $n$ th inverter respectively.

## V. VOLTAGE AND CURRENT DOUBLE LOOP CONTROL

In order to realize the tracking control of the reference's harmonic components of the outer voltage loop, hybrid control strategy combining P control and repetitive control is applied in the outer voltage loop, and P control is applied in the inner current loop. The voltage loop is realized in  $dq$  coordinate system, and the current loop is realized in  $\alpha\beta$  coordinate system.

Conventional hybrid control strategy combining P control and repetitive control is written as

$$G_{PRC}(s) = k_{vp} + k_{r1} \frac{e^{-sT_1}}{1 - Q_1 e^{-sT_1}} \quad (29)$$

where  $k_{vp}$  is the proportional coefficient of the voltage loop,  $k_{r1}$  is the gain of the repetitive control,  $T_1 = 2\pi/\omega$ , and  $Q_1$  is the internal mode coefficient of the repetitive control.

Expand (29) as follows

$$G_{PRC}(s) = k_{vp} - \frac{k_{r1}}{2Q_1} + \frac{k_{r1}}{T_1 Q_1 (s + \omega_{c1})} + \frac{2k_{r1}}{T_1 Q_1} \sum_{k=1}^{\infty} \frac{s + \omega_{c1}}{s^2 + 2\omega_{c1}s + \omega_{c1}^2 + (k\omega)^2} \quad (30)$$

where  $\omega_{c1}$  is the resonant bandwidth. The hybrid control combining P control and repetitive control can be equivalent to the parallel control of proportion, integral and each order quasi-resonance control, which has large gain at the fundamental and each order harmonic and realizes the tracking control of each order harmonic compensation.  $\omega_{c1} = -\ln Q_1/T_1$ . Reducing  $Q_1$  can increase  $\omega_{c1}$  to improve the stability of the

repetitive control, but also reduces the open-loop gain of the repetitive control leading to the increase of the tracking error of the repetitive control. For wider resonant bandwidth and larger open-loop gain of the repetitive control, it is necessary to increase  $k_{r1}$  and reduce  $Q_1$ . However,  $k_{r1}$  is related to the stability margin, and too large  $k_{r1}$  will lead to the system instability.  $Q_1$  is generally less than 1 and the capacity of microgrid is generally small, so the frequency error of the PCC voltage can be allowed within  $\pm 0.5\text{Hz}$  [21], then  $\omega_{c1} \leq \pi$  and  $Q_1$  is defined as 0.94.

According to (30), the repetitive control also has large gain at high frequency band, which affects the stability of the repetitive control. Low-pass filter is connected in series to improve the attenuation capability of the repetitive control to reduce the gain at high frequency band, and phase lead compensation is added to compensate phase to realize zero phase shift at middle and low frequency band as follows

$$G_{PRC}(s) = k_{vp} + k_{r1} \frac{e^{-sT_1}}{1 - Q_1 e^{-sT_1}} G_{LPF}(s) e^{sT_0 K_1} \quad (31)$$

where  $K_1$  is the phase lead compensation quantity, and  $T_0$  is the sampling period which is 0.1ms. According to Shannon's sampling theorem, the sampling frequency should be greater than twice the harmonic frequencies. Considering the delay of the control system,  $T_0$  can meet at least 50th order harmonic compensation.  $G_{LPF}(s)$  is the 2nd order low-pass filter as follows

$$G_{LPF}(s) = \frac{\omega_n^2}{s^2 + 2\xi\omega_n s + \omega_n^2} \quad (32)$$

where the cut-off frequency  $\omega_n$  is 2.6kHz, and the damping ratio  $\xi$  is 0.707.

In the three-phase AC circuit with nonlinear load, the positive sequence components are mainly  $6k + 1$ th order harmonics, and the negative sequence components are mainly  $6k - 1$ th order harmonics, where  $k$  is interger. When the three-phase voltage and current are transformed to the positive sequence fundamental  $dq$  coordinate system, the positive  $6k + 1$ th and negative sequence  $6k - 1$ th order harmonic components are all converted to  $6k$ th order harmonics. In order to improve the control gain of  $6k$ th order harmonics in  $dq$  coordinate system, FRC is added to (31) in parallel to obtain the MPRC strategy as follows

$$G_{PMRC}(s) = G_{PRC}(s) + k_{r2} \frac{e^{-sT_2}}{1 - Q_2 e^{-sT_2}} G_{LPF}(s) e^{sT_0 K_2} \quad (33)$$

where the repetitive control period of the FRC  $T_2 = T_1/6$ ,  $K_2$  is the phase lead compensation quantity,  $k_{r2}$  is the gain of the FRC and  $Q_2$  is the internal model coefficient of the FRC.

The MPRC is the parallel of the repetitive control with period  $T_1$  and the repetitive control with period  $T_1/6$ , and thus the performance of the repetitive control for tracking the reference signals of the integral multiples frequency harmonics of  $1/T_2$  in  $dq$  coordinate system is enhanced. The resonant bandwidth of the FRC  $\omega_{c2} = -\ln Q_2/T_2$ . To make the same

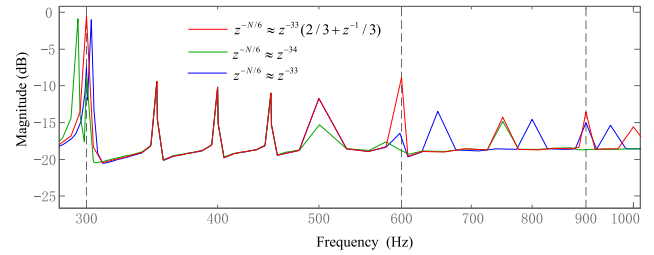


FIGURE 7. Magnitude-frequency characteristic curve of  $G_{PMRC}(z)$  at different values of  $z^{-N/6}$ .

resonant bandwidth of the two parallel repetitive controllers,  $Q_2 = \sqrt[6]{Q_1}$ . (33) is discretized as follows

$$G_{PMRC}(z) = k_{vp} + k_{r1} \frac{z^{-N}}{1 - Q_1 z^{-N}} G_{LPF}(z) z^{K_1} + k_{r2} \frac{z^{-N/6}}{1 - Q_2 z^{-N/6}} G_{LPF}(z) z^{K_2} \quad (34)$$

where  $N = T_1/T_0$ , and  $G_{LPF}(z)$  is the discretization of  $G_{LPF}(s)$ .

Only when  $N$  is divisible by 6, (34) can be implemented in the control system, but in the actual system  $N$  is not necessarily set to be integral multiples of 6. If  $z^{-N/6}$  is approximated as an adjacent integer of  $N/6$  order delay, the resonant frequencies of the FRC are different with the harmonic frequencies of the PCC voltage, and the tracking control performance of the main harmonic components is reduced. To solve this problem, the FRC adopts fractional order delay as follows

$$z^{-N/6} = z^{-m} z^{-F} \quad (35)$$

where  $m$  is an integer, and  $0 \leq F < 1$ . The fractional order delay  $z^{-F}$  can be approximated by the following Lagrange interpolation polynomial FIR filter

$$z^{-F} \approx \sum_{n=0}^x A(n) z^{-n} \quad (36)$$

$$A(n) = \prod_{\substack{i=0 \\ n \neq i}}^x \frac{F - i}{n - i} \quad i = 0, 1, \dots, x \quad (37)$$

To simplify the calculation, the value of  $x$  is defined as 1, and (36) is the linear interpolation as follows

$$z^{-F} \approx (1 - F) + F z^{-1} \quad (38)$$

when  $N = 200$ ,  $m = 33$  and  $F = 1/3$ . So  $z^{-N/6}$  is adjusted as

$$z^{-N/6} \approx z^{-33}(2/3 + z^{-1}/3) \quad (39)$$

Figure 7 is the magnitude-frequency characteristic curve of  $G_{PMRC}(z)$  at the main frequency band when  $z^{-N/6}$  is separately defined as  $z^{-33}$ ,  $z^{-34}$ , and  $z^{-33}(2/3 + z^{-1}/3)$ . From Figure 7, the open loop gain of  $z^{-N/6}$  as  $z^{-33}(2/3 + z^{-1}/3)$  is higher than that of  $z^{-N/6}$  as  $z^{-33}$  and  $z^{-34}$  at the

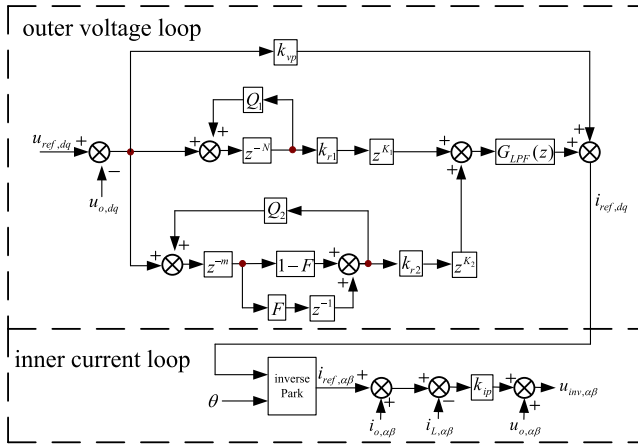


FIGURE 8. Control block diagram of the voltage and current double loop control.

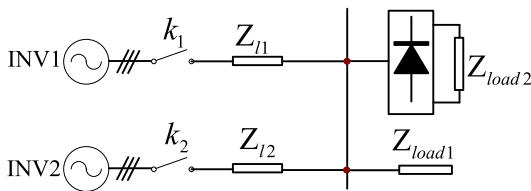


FIGURE 9. Islanded microgrid with nonlinear load.

frequencies 300Hz, 600Hz and 900Hz. So the fractional order delay proposed in this paper is necessary to improve the tracking control performance of the repetitive control at major harmonics. The MPRC can effectively improve the harmonic gains at middle and low frequency band for the tracking control performance of the given reference’s harmonic components of the voltage loop, especially 6kth order harmonics in dq coordinate system.

The control system block diagram of the voltage and current double loop control is shown in Figure 8.  $i_{ref,\alpha\beta}$ ,  $i_{o,\alpha\beta}$ ,  $i_{L,\alpha\beta}$ ,  $u_{o,\alpha\beta}$  and  $u_{inv,\alpha\beta}$  are the  $\alpha\beta$  components of  $i_{ref}$ ,  $i_o$ ,  $i_L$ ,  $u_o$  and  $u_{inv}$  respectively in  $\alpha\beta$  coordinate system.  $k_{ip}$  is the proportional coefficient of the current loop.

## VI. SIMULATION AND HIL TEST

### A. SIMULATION

The control strategy proposed in this paper is simulated and verified by simulation model in Matlab/Simulink. Figure 9 is the simulation model of the islanded microgrid with nonlinear load. INV1 and INV2 are connected in parallel, and the capacity ratio of them is 1:2. Table 1 is the main simulation parameters.  $Z_{load1}$  is the three-phase linear load. The DC side of the three-phase uncontrolled rectifier is connected with  $Z_{load2}$  to generate the nonlinear load.

When each phase of  $Z_{load1}$  is  $15\Omega$ , and  $Z_{load2}$  is  $40 + j\omega \times 0.03\Omega$ , the contrast of the harmonic contents of the PCC voltage by different control strategies is shown in Table 2, in which different control strategies: (a) Harmonic compensation loop is not applied and P control is applied in the outer

TABLE 1. Main simulation parameters.

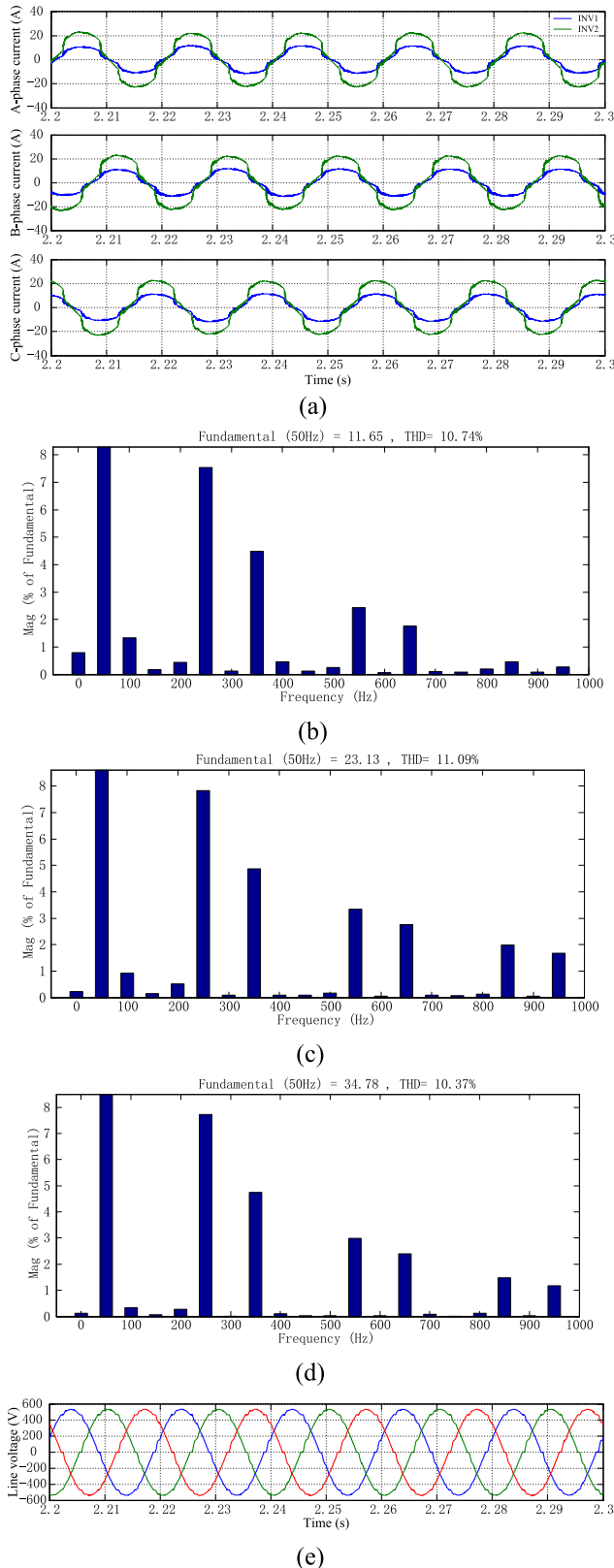
Parameter/unit	Numerical(INV1)	Numerical(INV2)
$L/\text{mH}$	4	2
$C/\mu\text{F}$	10	20
$Z_v^f/\Omega$	$0.3 + j\omega \times 0.006$	$0.15 + j\omega \times 0.003$
$R_v^h/\Omega$	7	3.5
$k_{ih}$	0.6	0.3
$Z_l^f/\text{m}\Omega$	$40 + j\omega \times 0.03$	$30 + j\omega \times 0.02$
$P_0/\text{kW}$	5	10
$Q_0/\text{kvar}$	2.5	5
$U_{dc}/\text{V}$		700
$U_0/\text{V}$		311
$\omega_0/(\text{rad/s})$		$100\pi$

TABLE 2. Contrast of the harmonic contents of the PCC voltage by different control strategies.

Control strategy	a	b	c	d
Fundamental (50Hz)/V	537.2	537.3	538.3	538.4
THD/%	6.22	3.75	3.24	2.59
Magnitude of each order harmonic/(% of fundamental)				
2nd	2.55	0.77	0.4	0.21
3rd	0.01	0.01	0.03	0.13
4th	2.03	0.59	0.35	0.4
5th	3.41	1.95	1.62	1.09
6th	0.03	0.01	0.03	0.14
7th	2.53	1.27	1.04	0.6
8th	0.57	0.17	0.12	0.02
9th	0.02	0.02	0.01	0.04
10th	0.3	0.08	0.1	0.04
11th	2.15	1.35	1.19	0.73
12th	0.04	0.02	0.02	0.11
13th	1.82	1.16	1.06	0.62
14th	0.19	0.15	0.14	0.13
15th	0.03	0.01	0.02	0.07
16th	0.1	0.22	0.21	0.22
17th	0.93	1.32	1.15	0.91
18th	0.04	0.01	0.05	0.09
19th	0.67	1.07	1.03	0.87

voltage loop; (b) Adaptive harmonic compensation control is applied and P control is applied in the outer voltage loop; (c) Adaptive harmonic compensation control is applied and (31) is applied in the outer voltage loop; (d) Adaptive harmonic compensation control is applied and (34) is applied in the outer voltage loop. The fundamental (50Hz) value is the fundamental magnitude of the 3-phase line voltage. By comparing (a) with (b) the adaptive harmonic compensation control can greatly improve the power quality of the islanded microgrid with nonlinear load. By comparing (b), (c) and (d), the harmonic gains improved by the MPRC at middle and low frequency band are good for the tracking control performance of the given reference’s harmonic components of the voltage loop, which can improve the ability of the control system to suppress the PCC voltage distortion, especially 5th, 7th, 11th, and 13th order harmonics.

By the control strategy presented in this paper, the current waveform of INV1 and INV2, the harmonic contents of the current of INV1, INV2 and the load, and the PCC voltage



**FIGURE 10.** Current waveform of INV1 and INV2, harmonic contents of the current of INV1, INV2 and the load, and PCC voltage waveform of the microgrid at steady state: (a) Output current of the inverters; (b) Harmonic contents of INV1's output current; (c) Harmonic contents of INV2's output current; (d) Harmonic contents of the load current; (e) PCC voltage of the microgrid.

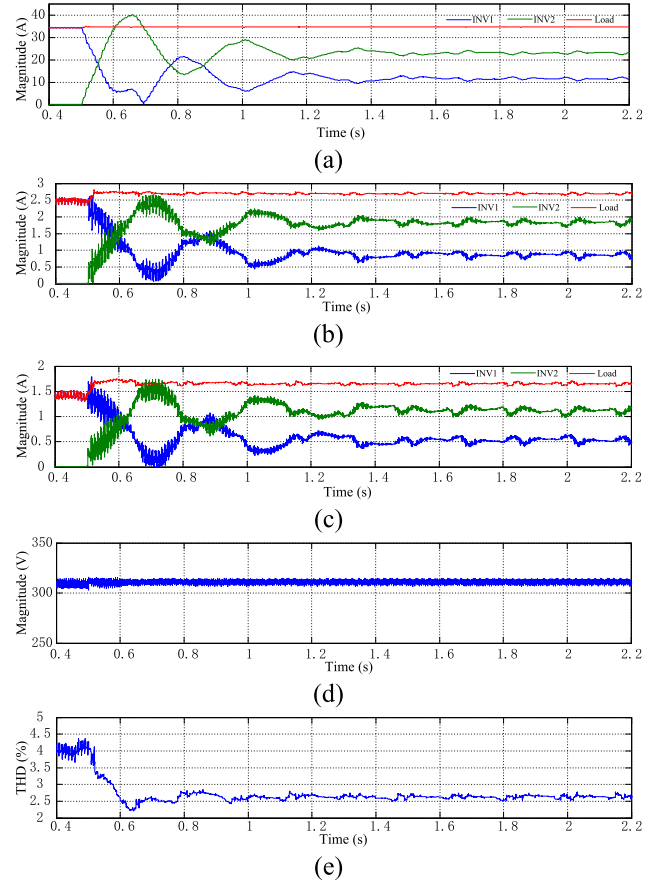


**FIGURE 11.** Waveform of the microgrid when the inverters are put into operation: (a) Magnitude of the fundamental current of the inverters and load; (b) Magnitude of the 5th order harmonic current of the inverters and load; (c) Magnitude of the 7th order harmonic current of the inverters and load; (d) Magnitude of the PCC voltage of the microgrid; (e) THD of the PCC voltage of the microgrid.

waveform of the microgrid at steady state are shown in Figure 10. The load condition of the microgrid is the same as that in Figure 10. The fundamental current magnitude of INV2 is nearly twice the fundamental current magnitude of INV1. The current of INV1 and INV2 have the same frequency and phase. The percentages of the main harmonic contents of the current among INV1, INV2 and the load are close. Figure 10 indicates that the control strategy has good steady performance and the harmonic circulation can be effectively suppressed.

The waveform of the microgrid when the inverters are put into operation is shown in Figure 11. Before  $t = 0.5$  s, only INV1 operates, and INV2 is put into operation at  $t = 0.5$  s. The load condition of the microgrid is the same as that in Figure 10. The current of the inverters changes smoothly and the PCC voltage is steady in the transient process. According to Figure 10(b), (c) and (d), the 5th and 7th order harmonics current is selected as main harmonics for analysis. The distribution ratio of the fundamental and main harmonics



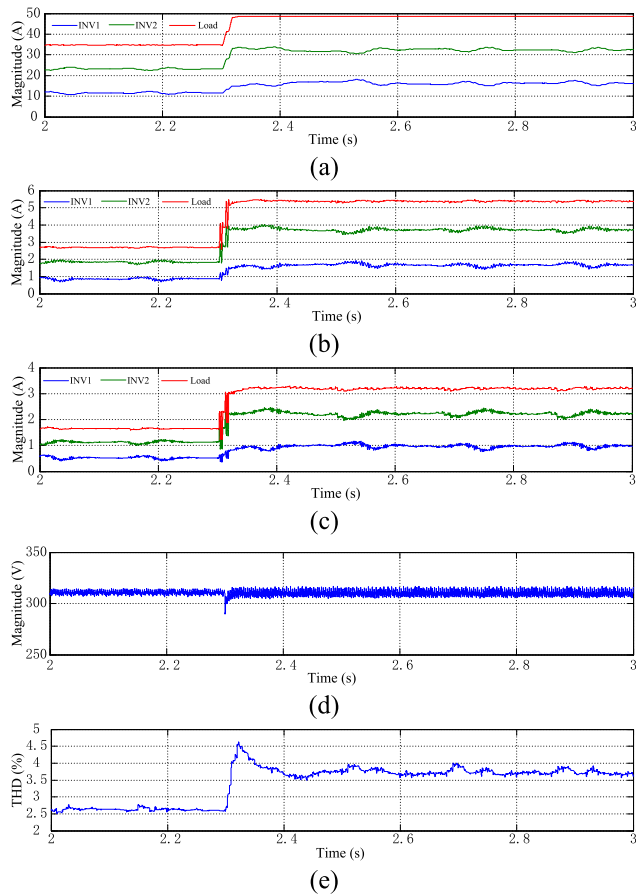


**FIGURE 12.** Waveform of the microgrid when the load suddenly changes: (a) Magnitude of the fundamental current of the inverters and load; (b) Magnitude of the 5th order harmonic current of the inverters and load; (c) Magnitude of the 7th order harmonic current of the inverters and load; (d) Magnitude of the PCC voltage of the microgrid; (e) THD of the PCC voltage of the microgrid.

current extracted by Fourier analysis is close to the ratio of the inverters' capacity.

The waveform when the load suddenly changes is shown in Figure 12. Each phase of  $Z_{load1}$  is  $15 \Omega$ . Before  $t = 2.3$  s  $Z_{load2}$  is  $40 + j\omega \times 0.03\Omega$ . At  $t = 2.3$  s  $Z_{load2}$  changes to  $20 + j\omega \times 0.015\Omega$  instantaneously. The current of the inverters changes smoothly, and the THD of the PCC voltage conforms to IEEE standard in the transient process. The distribution ratio of the current is close to the ratio of the inverters' capacity. The simulation results from Figure 11 and Figure 12 validate that the harmonic current distribution realized by  $R_v^h$  and  $k_{ih}$  is effective at various dynamic operating conditions.

**B. HIL TEST**

In order to further verify the proposed control strategy, the HIL real-time verification test based on Typhoon HIL604 is carried out. The microgrid model is established in Typhoon schematic editor and then download into HIL604 hardware platform. The islanded microgrid with nonlinear load of the HIL test system is as Figure 9. The

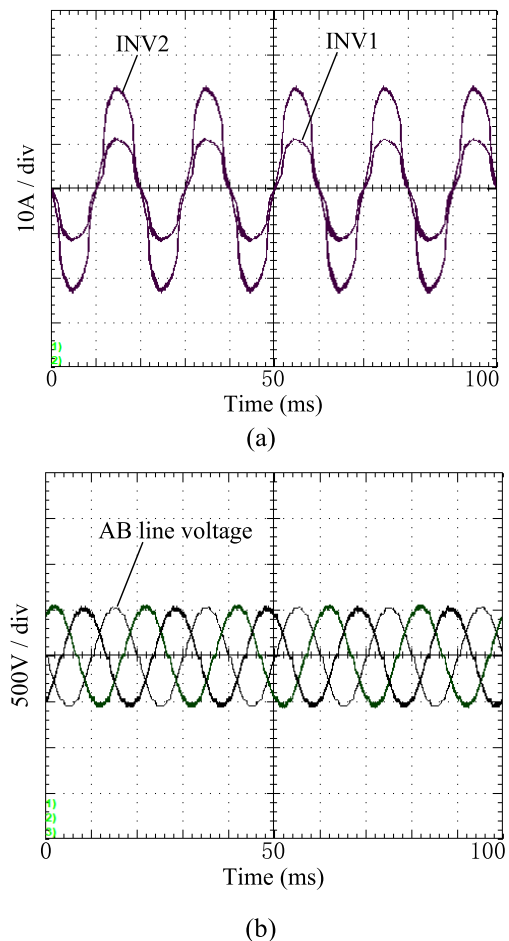


**FIGURE 13.** Current waveform of the inverters, and PCC voltage waveform of the microgrid at steady state: (a) A-phase output current of the inverters; (b) PCC voltage of the microgrid.

**TABLE 3.** Contrast of the inverters' output current.

	Case1		Case2	
	INV1	INV2	INV1	INV2
Fundamental magnitude/A	11.61	23.27	16.18	32.4
THD/%	10.67	9.59	14.65	13.24

parameters of the inverters and load are the same with those of the simulation presented in Table 1.

Case1: each phase of  $Z_{load1}$  is  $15 \Omega$  and  $Z_{load2}$  is  $40 + j\omega \times 0.03\Omega$ . Case2: each phase of  $Z_{load1}$  is  $15 \Omega$  and  $Z_{load2}$  is  $20 + j\omega \times 0.015\Omega$ . The current waveform of the inverters and the PCC voltage waveform of the microgrid at steady state are shown in Figure 13. The load condition of the microgrid is case1. The THD of the PCC voltage is 3.62%. The waveform when the load suddenly changes is shown in Figure 14. The load changes from case1 to case2 instantaneously. The current of the inverters changes smoothly and the PCC voltage is steady in the transient process. To demonstrate the fundamental and harmonic current distribution effect between the inverters, the contrast of the inverters' output current about the fundamental components and THD is given in Table 3.

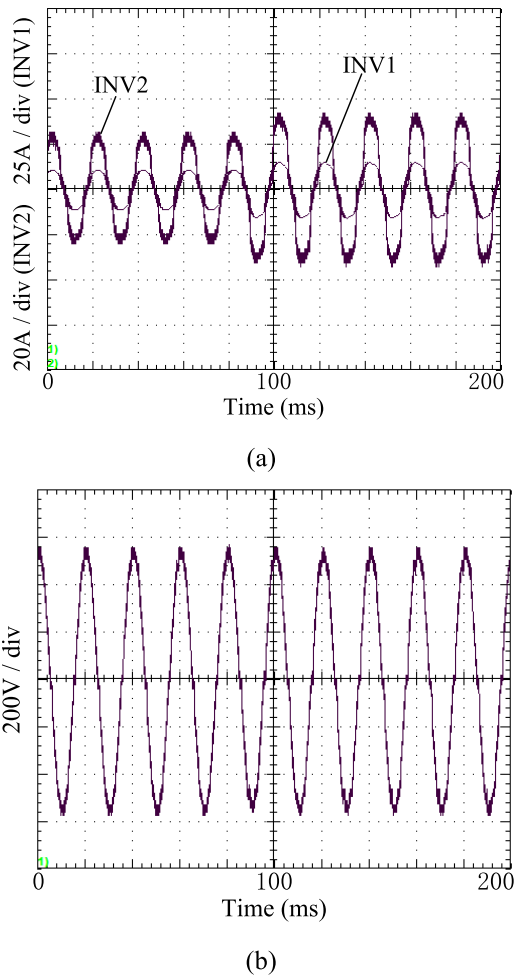


**FIGURE 14.** Current waveform of the inverters, and PCC voltage waveform of the microgrid when the load suddenly changes: (a) A-phase output current of the inverters; (b) AB line voltage of the PCC.

From Table 3, the distribution ratio of the fundamental and harmonic current is very close to the ratio of the inverters' capacity, and the current circulation is suppressed effectively.

## VII. CONCLUSION

In this paper, the power quality problems of islanded microgrid caused by nonlinear load are studied and addressed.

By analyzing the main circuit of the microgrid, the equivalent circuits in fundamental and harmonic domains are obtained, and then the generation mechanism of the harmonic circulation among the inverters and the PCC voltage harmonic distortion are deduced. According to the different control requirements of the fundamental and harmonic components of the inverters, the decoupling control of the fundamental and harmonic components is carried out. VSG control is applied in fundamental domain to realize the fundamental frequency and voltage regulation of the microgrid and the autonomous distribution of the fundamental current. Adaptive harmonic compensation and harmonic virtual impedance are used in harmonic domain against the PCC voltage har-

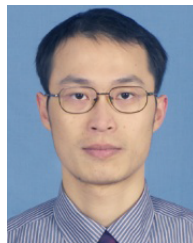
monic distortion and the harmonic circulation. The relationship among the adaptive compensation coefficient, harmonic virtual impedance, harmonic current and harmonic components of the PCC voltage is analyzed. Adaptive harmonic compensation can effectively overcome the shortcomings of virtual impedance. MPRC with FRC is used to improve the tracking control performance of the given reference's harmonic components of the voltage loop, especially the main harmonic components.

Simulation model is built in Matlab/Simulink for analysis and verification. The HIL real-time verification test based on Typhoon HIL604 is given. The simulation and HIL test results show that the control strategy proposed in this paper can effectively suppress the harmonic circulation and the PCC voltage distortion, which ensures the power quality of the microgrid. The control strategy has good steady and dynamic performance.

## REFERENCES

- [1] M. S. Mahmoud, S. A. Hussain, and M. A. Abido, "Modeling and control of microgrid: An overview," *J. Franklin Inst.*, vol. 351, no. 5, pp. 2822–2859, May 2014.
- [2] T. L. Vandoorn, J. D. M. De Koning, B. Meersman, and L. Vandevelde, "Review of primary control strategies for islanded microgrids with power-electronic interfaces," *Renew. Sustain. Energy Rev.*, vol. 19, pp. 613–628, Mar. 2013.
- [3] C.-C. Chang, D. Gorinevsky, and S. Lall, "Dynamical and voltage profile stability of inverter-connected distributed power generation," *IEEE Trans. Smart Grid*, vol. 5, no. 4, pp. 2093–2105, Jul. 2014.
- [4] Q. Liu, Y. Tao, X. Liu, Y. Deng, and X. He, "Voltage unbalance and harmonics compensation for islanded microgrid inverters," *IET Power Electron.*, vol. 7, no. 5, pp. 1055–1063, May 2014.
- [5] F. Chishti, S. Murshid, and B. Singh, "Development of wind and solar based AC microgrid with power quality improvement for local nonlinear load using MLMS," *IEEE Trans. Ind. Appl.*, vol. 55, no. 6, pp. 7134–7145, Dec. 2019.
- [6] G. Wang, X. Wang, and J. Lv, "An improved harmonic suppression control strategy for the hybrid microgrid bidirectional AC/DC converter," *IEEE Access*, vol. 8, pp. 220422–220436, 2020.
- [7] *IEEE Recommended Practice and Requirements for Harmonic Control in Electrical Power Systems*, IEEE Standard 519, 1992.
- [8] Z. Afshar, M. Mollayousefi, S. M. T. Bathaee, M. T. Bina, and G. B. Gharehpetian, "A novel accurate power sharing method versus droop control in autonomous microgrids with critical loads," *IEEE Access*, vol. 7, pp. 89466–89474, 2019.
- [9] Y. Sun, X. Hou, J. Yang, H. Han, M. Su, and J. M. Guerrero, "New perspectives on droop control in AC microgrid," *IEEE Trans. Ind. Electron.*, vol. 64, no. 7, pp. 5741–5745, Jul. 2017.
- [10] Y. Han and J.-I. Ha, "Droop control using impedance of grid-integrated DFIG within microgrid," *IEEE Trans. Energy Convers.*, vol. 34, no. 1, pp. 88–97, Mar. 2019.
- [11] G. W. Chang, C.-M. Yeh, and W.-C. Chen, "Meeting IEEE-519 current harmonics and power factor constraints with a three-phase three-wire active power filter under distorted source voltages," *IEEE Trans. Power Del.*, vol. 21, no. 3, pp. 1648–1654, Jul. 2006.
- [12] P. Sreekumar and V. Khadkikar, "A new virtual harmonic impedance scheme for harmonic power sharing in an islanded microgrid," *IEEE Trans. Power Del.*, vol. 31, no. 3, pp. 936–945, Jun. 2016.
- [13] B. Liu, Z. Liu, J. Liu, R. An, H. Zheng, and Y. Shi, "An adaptive virtual impedance control scheme based on small-AC-signal injection for unbalanced and harmonic power sharing in islanded microgrids," *IEEE Trans. Power Electron.*, vol. 34, no. 12, pp. 12333–12355, Dec. 2019.
- [14] P. Sreekumar and V. Khadkikar, "Direct control of the inverter impedance to achieve controllable harmonic sharing in the islanded microgrid," *IEEE Trans. Ind. Electron.*, vol. 64, no. 1, pp. 827–837, Jan. 2017.

- [15] C. Blanco, F. Tardelli, D. Reigosa, P. Zanchetta, and F. Briz, "Design of a cooperative voltage harmonic compensation strategy for islanded microgrids combining virtual admittance and repetitive controller," *IEEE Trans. Ind. Appl.*, vol. 55, no. 1, pp. 680–688, Feb. 2019.
- [16] T. V. Hoang and H.-H. Lee, "Virtual impedance control scheme to compensate for voltage harmonics with accurate harmonic power sharing in islanded microgrids," *IEEE J. Emerg. Sel. Topics Power Electron.*, early access, Mar. 26, 2020, doi: 10.1109/JESTPE.2020.2983447.
- [17] H. R. Baghaee, M. Mirsalim, G. B. Gharehpetan, and H. A. Talebi, "Nonlinear load sharing and voltage compensation of microgrids based on harmonic power-flow calculations using radial basis function neural networks," *IEEE Syst. J.*, vol. 12, no. 3, pp. 2749–2759, Sep. 2018.
- [18] J. He, B. Liang, Y. Wei Li, and C. Wang, "Simultaneous microgrid voltage and current harmonics compensation using coordinated control of dual-interfacing converters," *IEEE Trans. Power Electron.*, vol. 32, no. 4, pp. 2647–2660, Apr. 2017.
- [19] Z.-X. Zou, K. Zhou, Z. Wang, and M. Cheng, "Frequency-adaptive fractional-order repetitive control of shunt active power filters," *IEEE Trans. Ind. Electron.*, vol. 62, no. 3, pp. 1659–1668, Mar. 2015.
- [20] G. Pandove and M. Singh, "Robust repetitive control design for a three-phase four wire shunt active power filter," *IEEE Trans. Ind. Informat.*, vol. 15, no. 5, pp. 2810–2818, May 2019.
- [21] M. Tang, S. Bifaretti, S. Pipolo, S. Odhano, and P. Zanchetta, "A novel repetitive controller assisted phase-locked loop with self-learning disturbance rejection capability for three-phase grids," *IEEE J. Emerg. Sel. Topics Power Electron.*, vol. 8, no. 2, pp. 1870–1879, Jun. 2020.



**QIANG CHEN** received the B.S. degree in applied physics and the M.S. and Ph.D. degrees in electric machines and electric apparatus from Southeast University, Nanjing, China, in 2002, 2005, and 2009, respectively.

He is currently working as an Associate Professor with the Nanjing Institute of Technology, Nanjing. His current research interests include power electronics for microgrids, distributed generation, and energy storage systems.

• • •